Molecular Neurobiology (2019) 56:8018–8034
https://doi.org/10.1007/s12035-019-01658-x

Histone Deacetylases Contribute to Excitotoxicity-Triggered Degeneration of Retinal Ganglion Cells In Vivo

Annabelle Schlüter[1] · Bahar Aksan[1] · Rossella Fioravanti[2] · Sergio Valente[2] · Antonello Mai[2,3] · Daniela Mauceri[1]

Received: 1 March 2019 / Accepted: 20 May 2019 / Published online: 3 June 2019

Abstract

Excitotoxicity is known to modulate the nuclear accumulation, and thus activity state, of histone deacetylases (HDACs) in pyramidal neurons. In the retina, deregulation in activity and expression of different HDACs has been linked to pathological conditions such as retinitis pigmentosa, retinal ischemia, glaucoma, and acute optic nerve injury. Up to now, however, the effects of in vivo excitotoxicity on the different HDACs in retinal ganglion cells (RGCs) have not been thoroughly investigated. Here, we injected adult mice intravitreally with N-methyl-D-aspartate (NMDA) as a mean to trigger excitotoxicity-mediated RGC degeneration and we detected time-dependent loss of RGCs at 1 and 7 days after the insult. Further, we characterized the subcellular localization of HDACs belonging to class I (HDAC1, HDAC3), IIa (HDAC4, HDAC5, HDAC7, HDAC9), IIb (HDAC6, HDAC10), and IV (HDAC11) in RGCs. Our analyses revealed a differential pattern of HDACs nuclear distribution in RGCs following excitotoxicity. After 1 day, HDAC3, HDAC5, HDAC6, HDAC7, and HDAC11 showed altered subcellular localization in RGCs while 7 days after the excitotoxic insult, HDAC4 and HDAC9 were the only HDACs displaying changes in their subcellular distribution. Moreover, we found that in vivo selective inhibition of HDAC1/3 or HDAC4/5 via MS-275 (entinostat) or LMK-235, respectively, could prevent ongoing RGC degeneration. In conclusion, our results point towards a role of HDACs in RGC degeneration and identify HDAC1/3 and HDAC4/5 as potential therapeutic targets to treat degenerative retinal diseases.

Keywords Retinal ganglion cells · NMDA · Excitotoxicity · Histone deacetylase · Retinal degeneration · Neuroprotection

Introduction

Post-translational modifications of histone proteins can influence gene expression through different mechanisms [1]. Lysine acetylation is one of such modifications and is a reversible process catalyzed by histone acetyltransferases (HATs). Histone deacetylases (HDACs) mediate the removal of acetyl groups, which results in a denser chromatin structure generally associated with repression of gene transcription [1–3]. In mammals, several HDACs have been identified that differ in structure, enzymatic function, subcellular localization, phylogenetic properties, and expression patterns [4]. A first distinction can be made between classical HDACs, which are Zn^{2+}-dependent and subdivided into class I, II and IV, and the sirtuins family which represents class III and relies on NAD^{+} [3]. The class I HDAC family consists of HDAC1, HDAC2, HDAC3, and HDAC8. They are localized predominantly in the nucleus and possess a relatively simple structure consisting of the conserved deacetylase domain with short amino- and carboxy-terminal extensions. Class II is further subdivided into class IIa, which includes HDAC4, HDAC5, HDAC7, and HDAC9, and class IIb comprising HDAC6 and

Electronic supplementary material The online version of this article (https://doi.org/10.1007/s12035-019-01658-x) contains supplementary material, which is available to authorized users.

✉ Daniela Mauceri
Mauceri@nbio.uni-heidelberg.de

[1] Neurobiology, Interdisciplinary Center for Neurosciences, Heidelberg University, Im Neuenheimer Feld 366, 69120 Heidelberg, Germany

[2] Department of Drug Chemistry and Technologies, Sapienza University of Rome, Piazzale Aldo Moro 5, 00185 Rome, Italy

[3] Pasteur Institute, Cenci-Bolognetti Foundation, Sapienza University of Rome, Piazzale Aldo Moro 5, 00185 Rome, Italy

HDAC10. Class IIa HDACs have a large N-terminal domain with multiple phosphorylation sites acting as binding sites for chaperone protein 14-3-3 [5]. Class IIb HDACs are mainly localized in the cytoplasm [6, 7], have a different structure, and their function is less characterized. Up to now, the only identified member of class IV is HDAC11, which features a deacetylase domain homologous to class I and II with small N- and C-terminal extensions [4]. The subcellular localization of HDACs is not immutable. In non-neuronal cells, an export from the nucleus to the cytoplasm has been shown for HDAC1, HDAC3, and HDAC10 whereas a nuclear import has been demonstrated for HDAC6 [8–11]. Class IIa HDACs shuttling between the nucleus and cytoplasm is, however, the best characterized and takes place in a signal-dependent manner in different cell types [4, 12]. In neurons, nuclear-cytoplasmic shuttling of class IIa HDACs depends on synaptic activity and nuclear calcium signaling [13, 14].

Excitotoxicity is a pathological phenomenon in which an excess of calcium influx leads to neuronal death. N-Methyl-D-aspartate (NMDA) receptors (NMDARs) are the principal initiators of excitotoxic cell death induced either by high glutamate levels or NMDA exposure. NMDAR-mediated excitotoxicity has indeed been implicated in several neuropathological conditions [15]. In the eye, excitotoxicity has been linked to glaucoma, retinal ischemia, and diabetic retinopathy [16–20].

NMDARs can promote either neuronal survival or death depending on their subcellular localization. Synaptic NMDAR (sNMDAR) activation leads to synaptic plasticity and neuroprotection, while stimulation of extrasynaptic NMDARs (eNMDARs) causes cell death [15, 21]. At the genomic level, sNMDARs upregulate pro-survival genes and downregulate pro-death genes while eNMDARs do the opposite [22]. Further, shuttling between the cytosol and the nucleus of class IIa HDACs is differentially influenced by sNMDARs and eNMDARs; sNMDARs drive nuclear export of class IIa HDACs, while eNMDARs lead to their import into the nucleus [13, 14, 23].

The nuclear-cytoplasmic shuttling of HDACs has been reported under pathological conditions in different central nervous system areas including the retina [24–30]. However, in spite of the fact that HDACs have been identified as potential therapeutic targets in retinal disorders, a detailed picture of the subcellular localization of the different HDACs under pathological conditions is still lacking. Here, we triggered NMDA-induced excitotoxicity in vivo in the retina of adult mice and thoroughly characterized the subcellular localization of classical HDACs belonging to class I, IIa, IIb, and IV during RGC degeneration. Moreover, we investigated the capabilities of selective HDAC inhibitors to spare RGCs from ongoing degeneration. Our results reveal a role for HDACs during excitotoxicity and the potential of selective HDAC inhibition to protect RGCs from degeneration.

Methods

Animals

All experiments were performed in accordance with ethical guidelines imposed by the local governing body (Regierungspräsidium Karlsruhe, Germany). Adult 8-week-old male and female mice of the strain C57BL/6J (Charles River, Sulzfeld, Germany) were used in this study. Animals were maintained with food and water ad libitum on a regular 12 h light/dark cycle. After intravitreal injections, mice were kept under frequent observation to ensure animal welfare.

LMK-235 and MS-275 Synthesis

LMK-235 was prepared following synthetic procedures as reported in [31], while MS-275 was synthesized accordingly to the procedure described by our group [32], as follows.

Procedure for the synthesis of MS-275 (entinostat)

Triethylamine (1.93 mmol, 0.27 ml) and O-(Benzotriazol-1-yl)-N,N,N′,N′-tetramethyluronium tetrafluoroborate (0.58 mmol, 0.186 g) were added under nitrogen atmosphere to a solution of 4-(((pyridin-3-ylmethoxy)carbonylamino)methyl)benzoic acid (5) (0.48 mmol, 0.137 g) in dry N,N-dimethylformamide (5 ml), and the resulting mixture was stirred for 15 min. After this time, 1,2-phenylendiamine (0.48 mmol, 0.052 g) was added and stirring was continued for further 30 min. The reaction was quenched by water (20 ml), and the precipitate was filtered, washed with water (3 × 20 ml), and dried. The solid residue was purified by chromatography on silica gel 60 eluting with ethyl acetate to provide MS-275 as a colorless solid, which was recrystallized from acetonitrile: melting point 159–161 °C; yield 76.6%; 1H NMR (DMSO-d6) δ 4.24–4.25 (d, 2H, PhCH2), 4.85 (bs, 2H, NH2), 5.06 (s, 3-pyridyl-CH2), 6.54–6.56 (t, 1H, aniline proton), 6.73–6.75 (d, 1H, aniline proton), 6.91–6.95 (t, 1H, aniline proton), 7.12–7.14 (d, 1H, aniline proton), 7.32–7.7.39 (m, 3H, benzene protons and NHCOO), 7.74–7.76 (d, 1H, pyridine proton), 7.88–7.95 (m, 3H, benzene protons and pyridine proton), 8.50–8.51 (d, 1H, pyridine proton), 8.56 (s, 1H, pyridine proton), 9.58 (bs, 1H, PhCONH) ppm; 13C NMR (DMSO-d6) δ 44.3, 66.3, 118.4, 123.5, 124.1, 124.5, 124.8, 126.6, 127.4 (2C), 127.8 (2C), 133.2, 134.1, 135.6, 142.4, 143.9, 147.5, 148.2, 156.6, 167.0 ppm; MS (EI): m/z: 376.15 (M)+.

Intravitreal Injections

For intravitreal injections, mice were anesthetized by intraperitoneal injection of 0.3 mg/kg BW Medetomidine (Alvetra und Werfft GmbH, Vienna, Austria), 3 mg/kg BW Midazolam (Hameln Pharmaceuticals GmbH, Hameln, Germany), and 0.03 mg/kg BW Fentanyl (Janssen

Pharmaceutica, Beerse, Belgium) to induce deep anesthesia. To induce excitotoxicity in the retina, 20 nmol NMDA (Biotrend, Wangen/Zurich, Switzerland; 2 μl of 10 mM, dissolved in sterile 1xPBS), or 200 nmol glutamate (Sigma-Aldrich, St. Louis, Missouri, USA; 2 μl of 100 mM, dissolved in sterile 1xPBS) was injected in one eye with a 32-gauge needle (Nanofil syringe, 10 μl; World Precision Instruments, Sarasota, Florida, USA) under a stereomicroscope. The other eye received the same volume of 1xPBS (vehicle) as a control. After the injection, eyes were treated with eye ointment (Bepanthen; Roche, Basel, Switzerland). Afterwards, anesthesia was antagonized by 450 μg/kg BW Atipamezole (Prodivet pharmaceuticals S.A.; Raeren, Belgium), 0.3 mg/kg BW Flumazenil (Fresenius Kabi, Bad Homburg, Germany), and 0.7 mg/kg BW Narcanti/Naloxone (Inresa Arzneimittel GmbH, Freiburg, Germany). For retinal inhibition of HDACs, Tubastatin A, LMK-235, or MS-275 dissolved in DMSO were intravitreally co-injected with PBS or NMDA in a total volume of 2 μl. PBS- and NMDA-injected eyes received the same end-concentration of DMSO as vehicle (0.0125%). For combined experiments, LMK-235 and MS-275 were co-injected with PBS or NMDA in a total volume of 2 μl. PBS- and NMDA-injected eyes received the same end-concentration of DMSO as vehicle (0.025%). Studies carried out on cell cultures showed that effective HDAC inhibition using LMK-235 and MS-275 occurs when the concentration of the inhibitors is around 100 nM [33, 34]. The eye of an adult mouse has a volume of 4.4 ± 0.7 μl [35], and we injected 2 μl of volume, bringing the total volume to circa 6.4 μl. Thus, we injected 1 pmol of each inhibitor in order to achieve a concentration range of 150 nM taking into consideration that, most likely, the concentration of the inhibitors necessary to achieve effective in vivo inhibition would be higher than what is observed for cell culture (100 nM). For Tubastatin A, studies on cell cultures reported efficacy at 1 μM [36, 37]. We aimed at reaching an intravitreal concentration of 1.5 μM, which we achieved by injecting 9.6 pmol Tubastatin A in 2 μl of volume.

Tissue Preparation

Retinas were dissected 1 day (d1) or 7 days (d7) after intravitreal injections. For western blot analysis, animals were euthanized with CO_2; heads were decapitated and cooled in iced water. Eyes were enucleated, retinas were immediately dissected under a stereomicroscope and shock-frozen in liquid nitrogen. For histology, animals were euthanized by intraperitoneal injection with 400 mg/kg BW pentobarbital (Narcoren; Merial GmbH, Hallbergmoos, Germany), followed by a transcardial perfusion with ice-cold 1xPBS and 10% formalin for 5 min. Eyes were enucleated and post-fixed for 15 min. In order to dissect the retina, the cornea, iris, lens, and vitreous body were removed under a stereomicroscope. For the preparation of sagittal retina sections, the retina was kept in the surrounding sclera and pigment epithelium. Samples were embedded in Tissue-Tek® (Leica, Wetzlar, Germany), frozen and stored at − 80 °C until cryo-sectioning. For retina whole mount immunostainings, the retina was isolated from the sclera and pigment epithelium and transferred into PBS.

QRT-PCR Analysis

Total RNA was extracted from retinas using the RNeasy Mini Kit (Qiagen, Hilden, Germany) including an optional DNase I treatment at room temperature for 15 min according to the manufacturer's instructions (Qiagen, Hilden, Germany). Extracted RNA was reverse transcribed into first strand cDNA using High Capacity cDNA Reverse Transcription kit (Applied Biosystems, Foster City, California, USA). Quantitative reverse transcriptase PCR (QRT-PCR) was done on a StepOne plus Real Time PCR system using TaqMan Gene Expression Assays for the indicated genes (Applied Biosystems, Foster City, California, USA). The following TaqMan Gene Expression Assays were used in this study: *Thy1* (Mm01174153_m1), *Nefl* (Mm01315666_m1), *Ppia (*Mm02342430_g1), *Vegf* (Mm01281449_m1), *ActB* (Mm00607939_s1), *Atf3* (Mm00476032_m1), *Bdnf* (Mm00432069_m1), *Arc* (Mm00479619_g1). Expression of target genes was normalized against the expression of *Gapdh* (Mm99999915_g1), which was used as an endogenous control gene.

Western Blot Analysis

Retinas were homogenized in RIPA buffer (150 mM NaCl, 1% Triton X-100, 0.57% sodium deoxycholate, 0.1% SDS, 50 mM Tris, pH 8, 1x Complete™ cocktail of protease inhibitors, Roche). Homogenates were centrifuged with 13,000 rpm for 10 min. Supernatants were mixed with 4x Laemmli sample buffer (200 mM Tris/HCl pH 6.8, 8% SDS, 40% Glycerol, 50 mM EDTA, 0.08% bromophenol blue) and 1% dithiothreitol. Lysates were heated at 95 °C for 10 min. For SDS-PAGE, 20 μl of lysate was loaded (3.75% stacking gel; 15% resolving gel for proteins with molecular weight < 50 kDa, or 7% for molecular weights > 50 kDa). SDS-PAGE was performed at constant amperage (30 mA for stacking, 100 mA for separation) in running buffer (19 mM glycine, 2.5 mM Tris, 0.01% SDS). Protein transfer was performed on nitrocellulose paper membranes in transfer buffer (15 mM glycine, 2 mM Tris, 0.01% SDS, 20% methanol) at a constant voltage of 18 V for 2.5 h for proteins with molecular weight > 100 kDa, and for 1.5 h for molecular weights < 100 kDa. Membranes were blocked in 5% milk powder in 1xPBS-Tween 20 for 1 h at room temperature followed by an overnight incubation with primary antibodies at 4 °C. The following primary antibodies were used: rabbit-anti-GAPDH (1:20000 in 5% BSA, Cell Signaling Technology, 2118), goat-

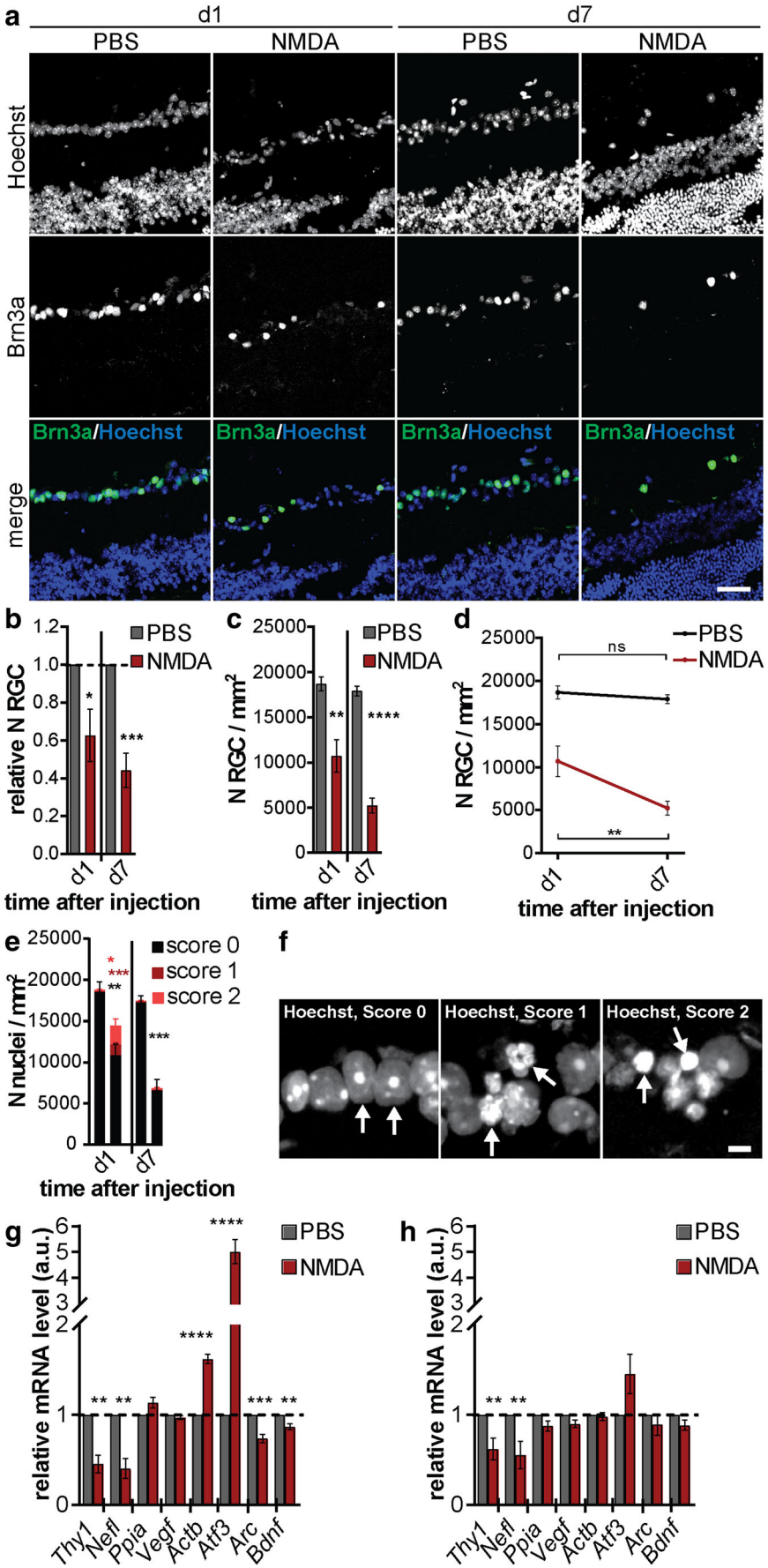
a
d1
d7
PBS
NMDA
PBS
NMDA
Hoechst
Brn3a
merge
Brn3a/Hoechst
b
relative N RGC
PBS
NMDA
time after injection
c
N RGC / mm²
time after injection
d
N RGC / mm²
ns
time after injection
e
N nuclei / mm²
score 0
score 1
score 2
time after injection
f
Hoechst, Score 0
Hoechst, Score 1
Hoechst, Score 2
g
relative mRNA level (a.u.)
Thy1
Nefl
Ppia
Vegf
Actb
Atf3
Arc
Bdnf
h
relative mRNA level (a.u.)

◀ **Fig. 1** NMDA-triggered excitotoxicity induces retinal ganglion cell death. **a** Representative images of sagittal retina sections at d1 and d7 after intravitreal injection of NMDA or PBS. RGCs were immunolabeled using Brn3a (green), and nuclei were labeled with Hoechst (blue). Scale bar = 40 μm. **b** Quantification of RGCs in retinas injected as indicated. RGC numbers in the NMDA-treated eye were normalized to the PBS control eye from the same animal. Unpaired *t* test. $n = 4$. PBS vs NMDA (d1), $p = 0.0355$; PBS vs NMDA (d7), $p = 0.0008$. **c** Quantification of RGCs in retinas injected as indicated. Unpaired *t* test. $n = 4$. PBS vs NMDA (d1), $p = 0.0064$; PBS vs NMDA (d7), $p < 0.0001$. **d** Time course analysis of progressive RGC death between d1 and d7 injected as indicated. Two-way ANOVA with Bonferroni's post hoc test for multiple comparisons. $n = 4$. PBS d1 vs d7, $p \geq 0.9999$; NMDA d1 vs d7, $p = 0.0079$. **e** Quantification of Hoechst-positive nuclei in the GCL injected as indicated. Nuclear morphology was classified into score 0 = healthy nuclei, score 1 = fragmented nuclei, and score 2 = condensed nuclei. Unpaired *t* test. $n = 4$. PBS vs NMDA (d1) score 0, $p = 0.0054$; PBS vs NMDA (d1) score 1, $p = 0.0008$; PBS vs NMDA (d1) score 2, $p = 0.0484$; PBS vs NMDA (d7) score 0, $p = 0.0005$; PBS vs NMDA (d7) score 1, $p = 0.4772$; PBS vs NMDA (d7) score 2, $p = 0.1891$. **f** Representative images of Hoechst-positive nuclei scored on a scale of 0–2 as described in **d**. Scale bar = 5 μm. **g** QRT-PCR analysis of *Thy1*, *Nefl*, *Ppia*, *Vegf*, *Actb*, *Atf3*, *Arc*, and *Bdnf* expression in the retinas of adult mice 1 day after intravitreal injection of NMDA. Unpaired *t* test. $n = 6$. *Thy1*, $p = 0.0025$; *Nefl*, $p = 0.0029$; *Ppia*, $p = 0.0714$; *Vegf*, $p = 0.0994$; *Actb*, $p < 0.0001$; *Atf3*, $p < 0.0001$; *Arc*, $p = 0.0002$; and *Bdnf*, $p = 0.0019$. **h** QRT-PCR analysis of *Thy1*, *Nefl*, *Ppia*, *Vegf*, *Actb*, *Atf3*, *Arc*, and *Bdnf* expression in the retinas of adult mice 7 days after intravitreal injection of NMDA. Unpaired *t* test. $n = 6$. *Thy1*, $p = 0.0249$; *Nefl*, $p = 0.0325$; *Ppia*, $p = 0.0675$; *Vegf*, $p = 0.0781$; *Actb*, $p = 0.6297$; *Atf3*, $p = 0.0942$; *Arc*, $p = 0.3862$; and *Bdnf*, $p = 0.0964$. Graphs represent mean ± SEM. $^{****}p < 0.0001$, $^{***}p < 0.001$, $^{**}p < 0.01$, $^{*}p < 0.05$

anti-Brn3a (1:1000 in 5% milk, Santa Cruz Biotechnology, sc-31984), rabbit-anti-HDAC3 (1:1000 in 5% BSA, Cell Signaling Technology, 2632), rabbit-anti-HDAC4 (1:6000 in 5% BSA, Cell Signaling Technology, 7628), rabbit-anti-HDAC5 (1:1000 in 5% BSA, 20458), rabbit-anti-HDAC6 (1:1000 in 5% milk, Abcam, ab1440). Secondary antibodies were incubated for 1 h at room temperature. The following secondary antibodies were used: peroxidase AffiniPure goat anti-rabbit IgG (H+L) (1:5000 in 5% milk, Jackson Immuno Research, DIanova, 111-035-144) and peroxidase AffiniPure donkey anti-goat IgG (H+L) (1:5000 in 5% milk, Jackson Immuno Research, DIanova, 705-035-147). Membranes were developed with enhanced chemiluminescence (ECL) solution (GE Healthcare AmershamTM) and the ChemiDoc Imaging System (BioRad).

For protein expression analysis in total retinal lysates, relative protein band densities were measured by using ImageJ/Fiji. Relative protein band densities were calculated by normalizing to the loading control (GAPDH). For each time point d1 and d7, relative protein levels of the NMDA-treated eyes were further normalized to relative protein levels of the PBS control eye of the same animal. Brn3a (RGCs marker) was used to monitor effective NMDA treatment. For all image analyses, backgrounds were subtracted. For each treatment, 3 animals were analyzed.

Cryo-sectioning

Sagittal retina sections of 15 μm thickness were obtained with a Leica CM1950 cryostat (Leica, Wetzlar, Germany) and mounted on superfrost plus slides (Thermo Scientific; Waltham, Massachusetts, USA). Slides were stored at − 20 °C until immunofluorescence.

Immunohistochemistry

Retinal sections were immunostained directly on microscope slides. Slides were incubated in 0.5% Triton-X100 and 10% fetal calf serum in 1xPBS for 1.5 h at room temperature. Primary antibodies were diluted in blocking solution and incubated overnight at 4 °C in a humidified chamber. For retinal whole mounts, free-floating immunostaining was performed. Retinas were blocked in 1% Triton-X100 and 10% fetal calf serum in 1xPBS overnight at 4 °C. Primary antibodies were diluted in blocking solution and incubated overnight at room temperature. The following antibodies were used: rabbit-anti-histone H3 (1:100; 06-755, Merck Millipore, Darmstadt, Germany), rabbit-anti-acetyl-histone H3 (Lys9) (1:500; 9649P, Cell Signaling Technology, Danvers, Massachusetts, USA), rabbit-anti-HDAC1 (1:100; PA1–860, Sigma-Aldrich, St. Louis, Missouri, USA), rabbit-anti-HDAC3 (1:100; 2632, Cell Signaling Technology, Danvers, Massachusetts, USA), rabbit-anti-HDAC4 (1:500; 7628S, Cell Signaling Technology, Danvers, Massachusetts, USA), rabbit-anti-HDAC5 (1:150; 20,458, Cell Signaling Technology, Danvers, Massachusetts, USA), rabbit-anti-HDAC6 (1:150; ab1440, Abcam, Cambridge, UK), rabbit-anti-HDAC7 (1:500; H2662, Sigma-Aldrich, St. Louis, Missouri, USA), rabbit-anti-HDAC9 (1:500; ab18970, Abcam, Cambridge, UK), rabbit-anti-HDAC10 (1:100; ab53096, Abcam, Cambridge, UK), rabbit-anti-HDAC11 (1:100; ab18973, Abcam, Cambridge, UK), and mouse-anti-Brn3a (1:500; sc-8429, Santa Cruz Biotechnology, Dallas, Texas, USA). For antibodies against H3 and HDACs HDAC3, HDAC5, HDAC6, HDAC7, HDAC9, HDAC10, and HDAC11, heat-induced epitope retrieval was performed prior to blocking by incubating the slides in pre-heated sodium citrate buffer (10 mM sodium citrate, 0.05% Tween 20, pH 6.0) at 95 °C for 10 min. After primary antibody incubation, the samples were washed and incubated with secondary antibodies in blocking solution for 1.5 h at room temperature (for sagittal sections) or overnight at 4 °C (for whole mounts). The following secondary antibodies were used: goat-anti-rabbit IgG (H+L) Alexa Fluor 488 (1:1000; A11008, Life Technologies, Carlsbad, California, USA) and goat-anti-mouse IgG (H+L) Alexa Fluor 594 (1:1000; A11005, Life Technologies, Carlsbad, California, USA). Nuclei were labeled with Hoechst (1:6000 in 1xPBS, Serva Electrophoresis GmbH, Heidelberg, Germany) for 10 min.

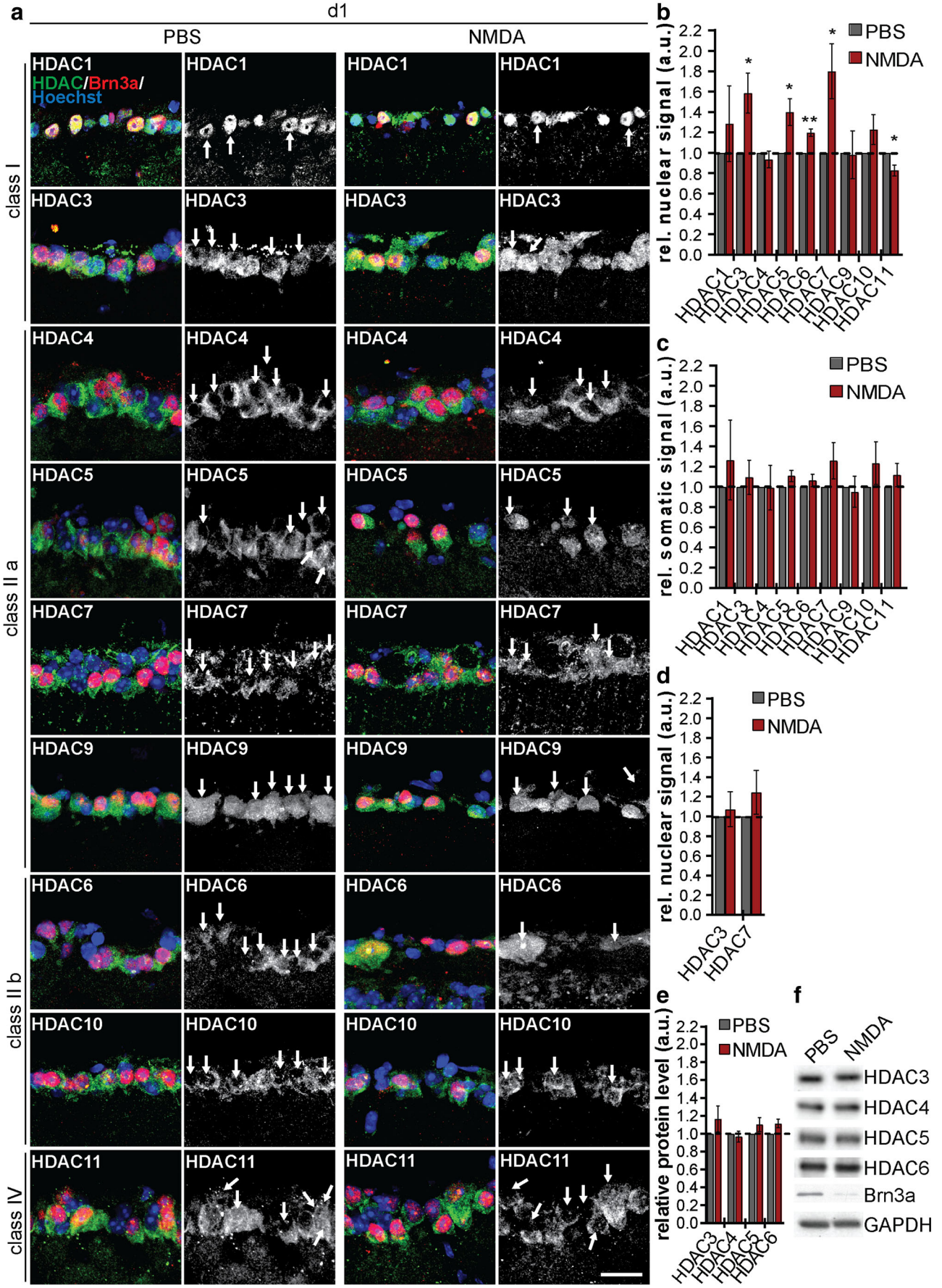
a
d1
PBS
NMDA
HDAC1
HDAC/Brn3a/
Hoechst
HDAC3
HDAC4
HDAC5
HDAC7
HDAC9
HDAC6
HDAC10
HDAC11
class I
class II a
class II b
class IV
b
rel. nuclear signal (a.u.)
PBS
NMDA
HDAC1
HDAC3
HDAC4
HDAC5
HDAC6
HDAC7
HDAC9
HDAC10
HDAC11
c
rel. somatic signal (a.u.)
d
rel. nuclear signal (a.u.)
e
relative protein level (a.u.)
f
PBS
NMDA
HDAC3
HDAC4
HDAC5
HDAC6
Brn3a
GAPDH

◀ **Fig. 2** NMDA-triggered excitotoxicity mediates subcellular relocation of histone deacetylases in retinal ganglion cells at d1. **a** Representative images of sagittal retina sections at d1 after intravitreal injections of NMDA or PBS. HDAC labeling is shown in green. Brn3a labeling, indicative of RGCs, is shown in red. Nucleus labeling (Hoechst) is shown in blue. Arrows indicate the location of nuclei of Brn3a-positive RGCs. Scale bar = 40 μm. **b** Quantification of nuclear HDAC signals in Brn3a-positive cells in retinas of mice injected as indicated. HDAC values in the NMDA-treated eye were normalized to the PBS control eye from the same animal. Unpaired *t* test. $n = 3$–4. HDAC1, $p = 0.4868$; HDAC3, $p = 0.0400$; HDAC4, $p = 0.4657$; HDAC5, $p = 0.0379$; HDAC6, $p = 0.0015$; HDAC7, $p = 0.0400$; HDAC9, $p = 0.9397$; HDAC10, $p = 0.1740$; HDAC11, $p = 0.0327$. **c** Quantification of somatic HDACs signals in Brn3a-positive cells in retinas of mice injected as indicated. HDAC values in the NMDA-treated eye were normalized to the PBS control eye from the same animal. Unpaired *t* test. $n = 3$–4. HDAC1, $p = 0.5386$; HDAC3, $p = 0.6015$; HDAC4, $p = 0.9714$; HDAC5, $p = 0.1251$; HDAC6, $p = 0.3288$; HDAC7, $p = 0.2207$; HDAC9, $p = 0.7637$; HDAC10, $p = 0.3026$; HDAC11, $p = 0.3641$. **d** Quantification of HDAC signals in nuclei of cells located in the INL in retinas of mice injected as indicated. HDAC values in the NMDA-treated eye were normalized to the PBS control eye from the same animal. Unpaired *t* test. $n = 3$. HDAC3, $p = 0.7030$; HDAC7, $p = 0.3342$. **e** Quantification of protein levels of HDAC3, HDAC4, HDAC5, and HDAC6 in retinal lysates of mice injected as indicated. Protein levels in the NMDA-treated eye were normalized to the PBS control eye from the same animal. Unpaired *t* test. $n = 4$. HDAC3, $p = 0.3016$; HDAC4, $p = 0.6167$; HDAC5, $p = 0.2267$; HDAC6, $p = 0.0556$. F) Representative immunoblots of the quantifications displayed in **e**. Graphs represent mean ± SEM. $^{**}p < 0.01$, $^{*}p < 0.05$

Image Acquisition

For each analysis, images were acquired with constant microscopy settings (exposure time, pixel size, bit depth, binning) across experiments. For each experiment, all images were acquired on the same day to avoid possible variations in fluorescence lamp excitation. Images of retinal sections were acquired in the central part of the retina. Images of retinal sections and whole mounts were acquired with Leica DM IRBE inverted fluorescent microscope with a × 40 oil immersion objective (Leica, Wetzlar, Germany) and a Spot Insight FireWire 2 camera with VisiView software (Visitron Systems GmbH, Diagnostic Instruments, Puchheim, Germany); with a Nikon A1R confocal laser scanning microscope (at the Nikon Imaging Center of Heidelberg University, Germany) with a × 40 oil immersion objective (Nikon, Minato, Tokyo, Japan); or with a Leica SP8 confocal laser scanning microscope with a × 63 oil immersion objective (Leica, Wetzlar, Germany).

Quantification of RGCs

For RGC number quantification in sagittal retina sections, Brn3a-positive and Hoechst-labeled cells located in the ganglion cell layer (GCL) were manually counted in 8 images using ImageJ/Fiji. Each image corresponds to one individual 15 μm sagittal retina section. For RGC number quantification in retinal whole mounts, Brn3a-positive cells were manually counted in 8 images per retina equally acquired in the central and peripheral part of the retina using ImageJ/Fiji. For each eye, RGC number was summed and normalized to the analyzed area. Relative RGC numbers at d1 and d7 were calculated by normalizing RGC numbers in the NMDA-treated eyes to the mean number of RGCs in the PBS-treated eyes at d1. For each treatment, 4 animals were analyzed.

Scoring of Nuclear Morphology

Nuclear morphology of cells in the GCL was scored on a scale of 0–2. Score 0 indicated cells with healthy euchromatic nuclei and normally formed nucleoli; score 1 indicated cells with fragmented nuclei; score 2 indicated cells with completely condensed pyknotic chromatin. For each score, nuclei were manually counted in 8 images, each corresponding to one individual 15 μm sagittal retina section using ImageJ/Fiji. For each eye, numbers of nuclei were summed and normalized to the analyzed area. For each treatment, 4 animals were analyzed.

Analysis of Fluorescence Intensity

Nuclear levels of H3, AcH3, and HDACs in sagittal retina sections were analyzed as previously published [14, 23, 38]. Fluorescent signals were measured in manually drawn regions of interest in single Brn3a-positive RGC nuclei in 5 images, each corresponding to one individual 15 μm sagittal retina section using ImageJ/Fiji. Nuclear HDAC levels were additionally measured in cells located in the inner nuclear layer (INL) as described above. Mean values were calculated from single nuclei values for each NMDA-treated eye and normalized to the mean value of the PBS-treated eye of the same animal. For quantification of somatic levels of HDACs in sagittal retina sections, fluorescent signals were measured in manually drawn regions of interest in Brn3a-positive cells located in the GCL using ImageJ/Fiji. Mean values were calculated for each NMDA-treated eye and normalized to the mean value of the PBS-treated eye as well as to the number of Brn3a-positive nuclei of the same animal. Background subtraction was performed prior to all analyses. Cells or nuclei that were overlapping other cells/nuclei were excluded from analyses to avoid hampering of results. For each treatment, 3–4 animals were analyzed.

For quantification of nuclear AcH3 levels in retinal whole mounts, integrated densities of fluorescent signals were measured in regions of interest of the same size in 8 pictures equally acquired in the central and peripheral part of the retina using ImageJ/Fiji. For each analyzed time point (d1 and d7), mean values were calculated for each NMDA-treated eye and normalized to the mean value in the PBS-treated eyes at d1

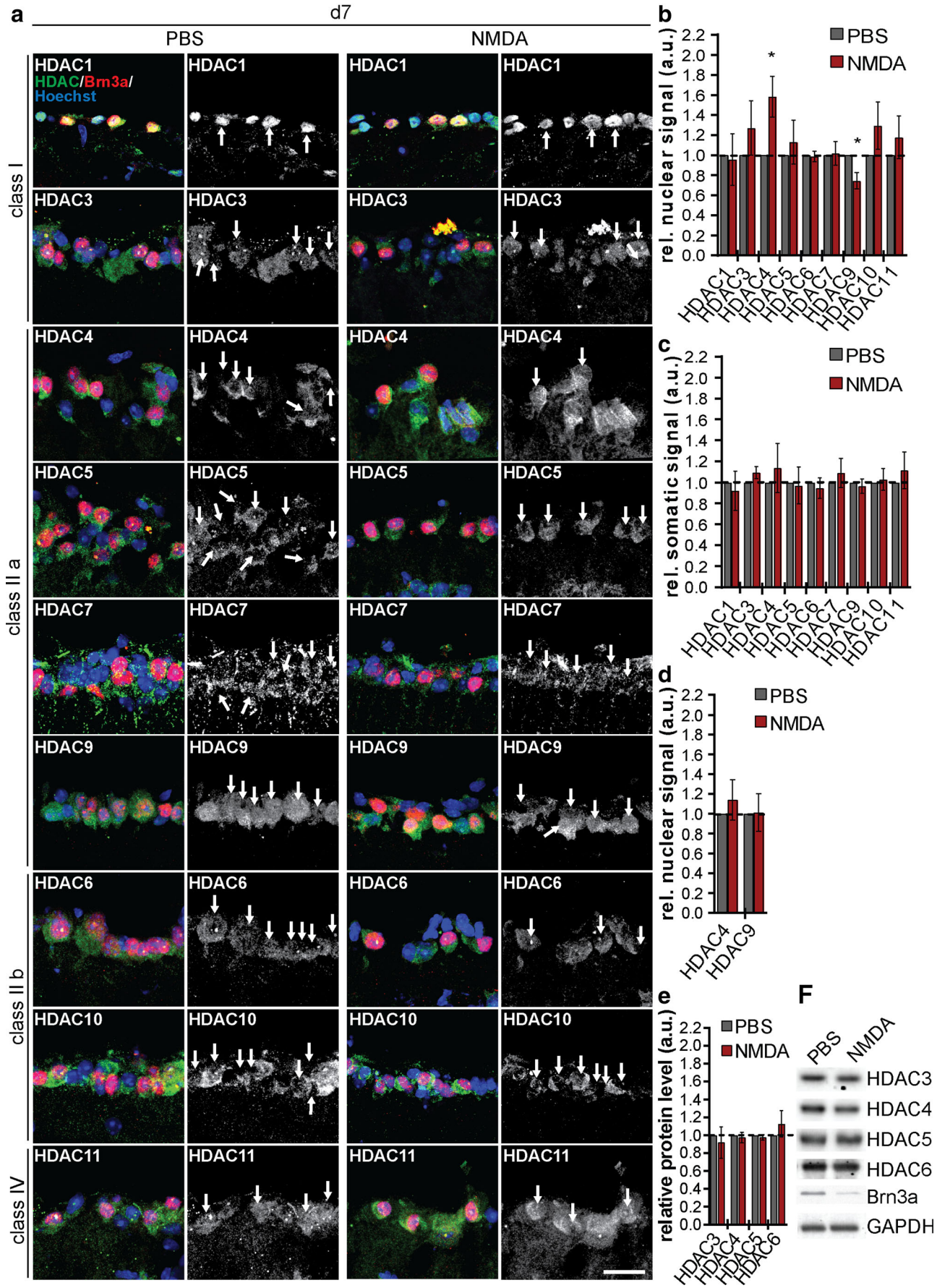
a
d7
PBS
NMDA
class I
class II a
class II b
class IV
HDAC1
HDAC/Brn3a/
Hoechst
HDAC3
HDAC4
HDAC5
HDAC7
HDAC9
HDAC6
HDAC10
HDAC11
b
rel. nuclear signal (a.u.)
PBS
NMDA
HDAC1
HDAC3
HDAC4
HDAC5
HDAC6
HDAC7
HDAC9
HDAC10
HDAC11
c
rel. somatic signal (a.u.)
d
rel. nuclear signal (a.u.)
e
relative protein level (a.u.)
F
PBS
NMDA
HDAC3
HDAC4
HDAC5
HDAC6
Brn3a
GAPDH

◀ **Fig. 3** NMDA-triggered excitotoxicity mediates subcellular relocation of histone deacetylases in retinal ganglion cells at d7. **a** Representative images of sagittal retina sections at d7 after intravitreal injections of NMDA or PBS. HDAC labeling is shown in green. Brn3a labeling, indicative of RGCs, is shown in red. Nuclei labeling (Hoechst) is shown in blue. Arrows indicate the location of nuclei of Brn3a-positive RGCs. Scale bar = 40 μm. **b** Quantification of nuclear HDAC signals in Brn3a-positive cells in retinas of mice as indicated. HDAC values in the NMDA-treated eye were normalized to the PBS control eye from the same animal. Unpaired *t* test. $n = 3$–4. HDAC1, $p = 0.8635$; HDAC3, $p = 0.3755$; HDAC4, $p = 0.0450$; HDAC5, $p = 0.5830$; HDAC6, $p = 0.7985$; HDAC7, $p = 0.8949$; HDAC9, $p = 0.0317$; HDAC10, $p = 0.2590$; HDAC11, $p = 0.4552$. **c** Quantification of somatic HDAC signals in Brn3a-positive cells in retinas of mice injected as indicated. HDAC values in the NMDA-treated eye were normalized to the PBS control eye from the same animal. Unpaired *t* test. $n = 3$–4. HDAC1, $p = 0.6850$; HDAC3, $p = 0.1758$; HDAC4, $p = 0.5771$; HDAC5, $p = 0.8698$; HDAC6, $p = 0.5944$; HDAC7, $p = 0.5586$; HDAC9, $p = 0.6421$; HDAC10, $p = 0.7891$; HDAC11, $p = 0.5449$. **d** Quantification of HDAC signals in nuclei of cells located in the INL in retinas of mice injected as indicated. HDAC values in the NMDA-treated eye were normalized to the PBS control eye from the same animal. Unpaired *t* test. $n = 3$. HDAC4, $p = 0.5313$; HDAC9, $p = 0.9498$. **e** Quantification of protein levels of HDAC3, HDAC4, HDAC5, and HDAC6 in retinal lysates of mice injected as indicated. Protein levels in the NMDA-treated eye were normalized to the PBS control eye from the same animal. Unpaired *t* test. $n = 4$. HDAC3, $p = 0.6563$; HDAC4, $p = 0.6845$; HDAC5, $p = 0.4953$; HDAC6, $p = 0.4157$. **f** Representative immunoblots of the quantifications displayed in **e**. Graphs represent mean ± SEM. $^{*}p < 0.05$

and d7, respectively. Background subtraction was performed prior to analysis. For each treatment, 4 animals were analyzed.

Statistical Analysis

Mean values and standard error of the mean (SEM) were calculated in Excel (Microsoft), and plotted and analyzed in GraphPad Prism 7 software (GraphPad Software, Inc.). Values were tested for normal distribution by performing a Shapiro-Wilk normality test. Unpaired *t* test and one-way or two-way analysis of variance (ANOVA) with Bonferroni's post hoc test for multiple comparisons were used. Details on the test used and *N* of each experiment are indicated in the respective figure legends. Bars represent mean values. Error bars indicate SEM. Asterisks indicate significant differences ($^{****}p < 0.0001$, $^{***}p < 0.001$, $^{**}p < 0.01$, $^{*}p < 0.05$).

Results

NMDA-Triggered Excitotoxicity Induces Retinal Ganglion Cell Death

Retinal ganglion cells (RGCs) are particularly sensitive to high glutamate and NMDA exposure in vitro and in vivo [39–43]. We employed a single intravitreal injection of 20 nmol NMDA in adult mice to trigger RGC degeneration (Fig. 1) and analyzed NMDA-induced excitotoxic RGC death at two different time points (day 1 (d1) and day 7 (d7)) after NMDA intravitreal delivery. Brn3a was used as a marker to identify RGCs [44]. Loss of RGCs occurred quickly; 1 day after NMDA intravitreal injection, the number of RGCs was significantly decreased in comparison with the control PBS-injected eyes (Fig. 1a–c; d1). At this time point, a significantly higher number of fragmented and condensed nuclei were present (Fig. 1e, f; d1, score 1–2) [30, 45]. RGC degeneration significantly worsened over time as observed 7 days after the NMDAR-mediated insult (Fig. 1a–d; d7). The remaining surviving cells in the GCL mainly exhibited healthy euchromatic nuclei with normally formed nucleoli (Fig. 1e; d7, score 0). We analyzed the mRNA level of a panel of 8 genes on retina homogenates at 1 and 7 days after NMDA intravitreal injection. At both d1 and d7, we detected a significant reduction in the mRNA level of the RGCs markers *Thy1* and *Nefl* (Fig. 1g, h). We additionally analyzed expression levels of *Pp1a* (housekeeping), *Vegf* (marker for potential injury-induced angiogenesis), *Actb* (cytoskeleton), *Atf3* (transcription factor), and *Arc* and *Bdnf* (activity-regulated immediately early genes). At d1 after NMDA-induced toxicity, *Actb* and *Atf3* mRNA levels were increased while mRNA levels of *Arc* and *Bdnf* were reduced (Fig. 1g). At d7, the only affected genes by NMDA-mediated injury remained the RGC markers *Thy1* and *Nefl* (Fig. 1h). None of the other analyzed genes showed statistically significant changes in their mRNA levels (Fig. 1h). Collectively, these data confirm that NMDA causes robust and time-dependent degeneration of RGCs in vivo.

NMDA-Triggered Excitotoxicity Differentially Modulates the Nuclear Content of HDACs in Retinal Ganglion Cells In Vivo

Excitotoxicity triggers nuclear accumulation of class IIa HDACs in pyramidal neurons [13, 23]. In the retina, activity of HDACs has been linked to pathological conditions [46, 47]. We analyzed the subcellular localization of HDAC1 and HDAC3 (class I); HDAC4, HDAC5, HDAC7, and HDAC9 (class IIa); HDAC6 and HDAC10 (class IIb); and HDAC11 (class IV) following NMDA-triggered excitotoxicity. The subcellular localization of HDAC2 and HDAC8 was not analyzed due to technical limitations and non-expression in the retina [48], respectively. In control conditions, HDAC3, HDAC9, and HDAC11 were localized to both the nucleus and cytoplasm of RGCs (Figs. 2 and 3). HDAC1 was mainly localized to the nucleus while HDAC4, HDAC5, HDAC6, HDAC7, and HDAC10 displayed a predominant localization to the cytoplasm of RGCs (Figs. 2 and 3). We specifically quantified the nuclear levels of HDACs in Brn3a-positive RGCs. At d1 after intravitreal NMDA injections, we detected a

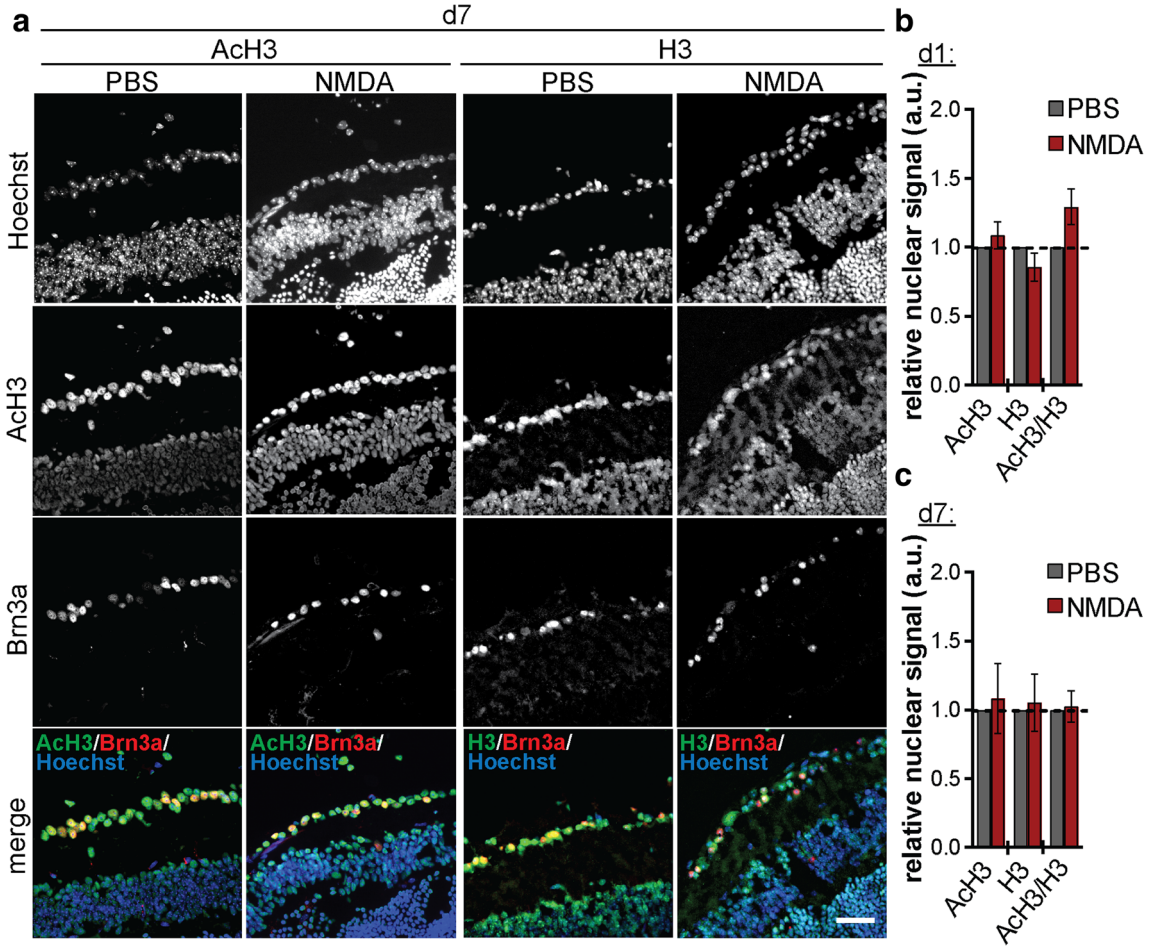

Fig. 4 NMDA-triggered excitotoxicity does not change histone acetylation in retinal ganglion cells. **a** Representative images of sagittal retina sections at d7 after intravitreal injections of NMDA or PBS. AcH3 (left columns) or H3 (right columns) labeling is shown in green. Brn3a labeling, indicative of RGCs, is shown in red. Nucleus labeling (Hoechst) is shown in blue. Scale bar = 40 μm. **b** Quantification of AcH3 and H3 signals in RGCs at d1 injected as indicated. AcH3 and H3 levels in the NMDA-treated eye were normalized to the PBS control eye from the same animal. Unpaired *t* test. $n = 3$. AcH3, $p = 0.4274$; H3, $p = 0.2277$; Ach3/H3, $p = 0.0877$. **c** Quantification of Ach3 and H3 signals in RGCs at d7 injected as indicated. AcH3 and H3 levels in the NMDA-treated eye were normalized to the PBS control eye from the same animal. Unpaired *t* test. $n = 3$. AcH3, $p = 0.7635$; H3, $p = 0.8109$; Ach3/H3, $p = 0.8399$. Graphs represent mean ± SEM

significant increase of nuclear levels of HDAC3, HDAC5, HDAC6, and HDAC7, as well as a significant decrease of nuclear levels of HDAC11 (Fig. 2a, b). We additionally quantified somatic levels of the different HDACs in Brn3a-positive RGCs (Fig. 2c). These analyses did not reveal any changes in the somatic expression of HDACs suggesting that the increased or decreased nuclear levels are most likely due to subcellular redistribution and not to changes in their expression level. To test whether this subcellular redistribution specifically occurred in RGCs, we additionally measured nuclear HDAC levels in cells of the inner nuclear layer (INL) (Fig. 2d). Nuclear levels of HDAC3 and HDAC7, which displayed the highest nuclear increase after intravitreal NMDA injections in RGCs at d1, did not show any changes in cells located in the INL (Fig. 2d). Moreover, total protein levels in retinal lysates of HDAC3, HDAC4, HDAC5, and HDAC6 were unaffected by NMDA-triggered excitotoxic RGC death at d1 (Fig. 2e).

We carried out similar analyses 7 days (d7) after NMDA-triggered excitotoxicity (Fig. 3). In agreement with what was observed at d1, somatic levels of the analyzed HDACs in Brn3a-positive RGCs were not changed (Fig. 3c). However, the nucleo-cytoplasmic HDAC redistribution observed at d1 after NMDA-induced excitotoxicity was no longer present. Rather, we detected a different pattern of HDAC nucleo-cytoplasmic distribution. We found nuclear HDAC4 levels to be significantly increased and nuclear HDAC9 levels to be decreased (Fig. 3a, b). In the INL, nuclear levels of these HDACs were unchanged (Fig. 3d). Further, retinal protein levels of HDAC3, HDAC4, HDAC5, and HDAC6 remained stable at d7 after intravitreal NMDA injections (Fig. 3e).

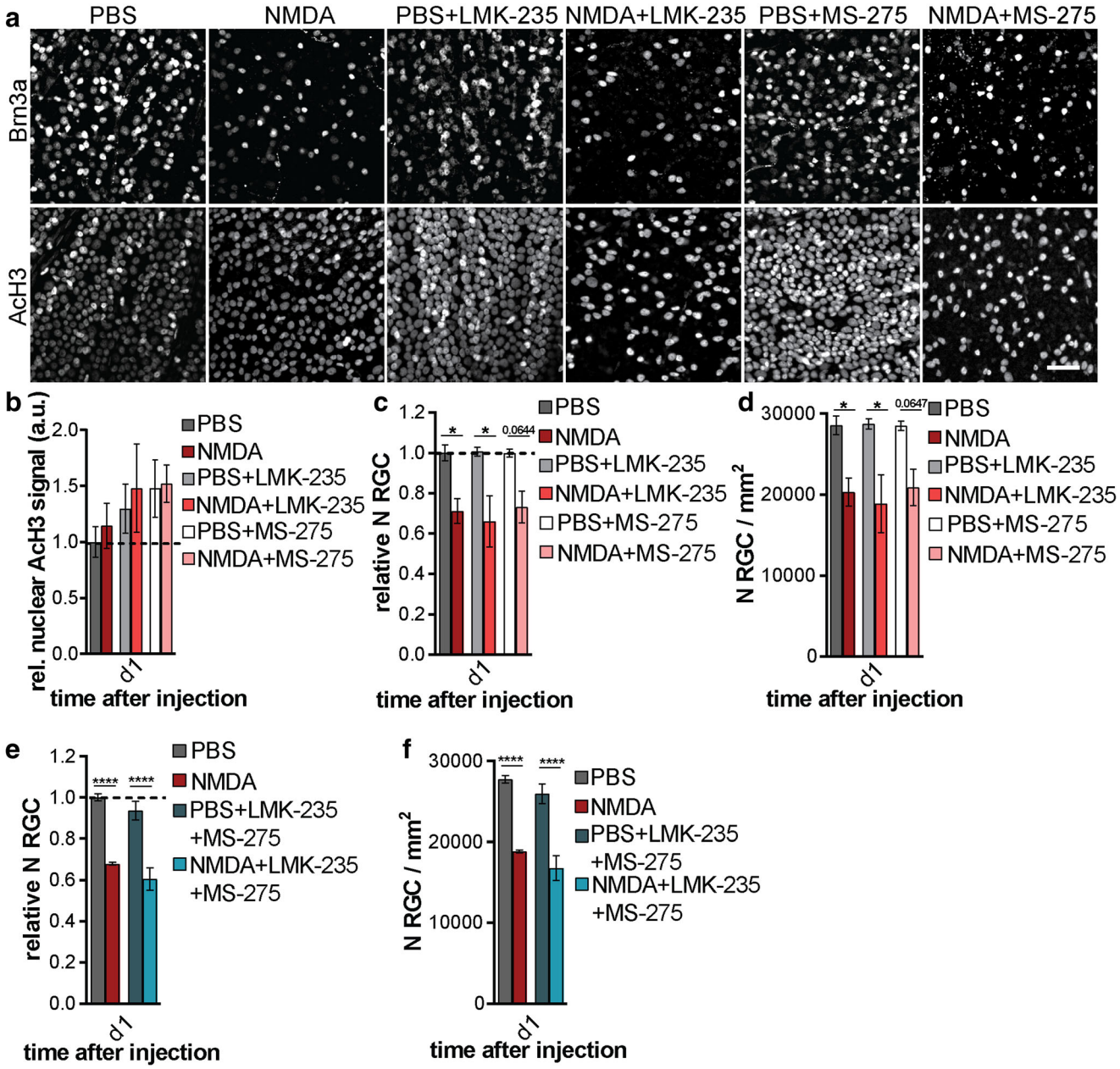

Fig. 5 HDAC inhibition does not affect excitotoxic retinal ganglion cell death at d1. **a** Representative images of retinal whole mounts at d1 after intravitreal injections of NMDA/PBS, NMDA/PBS+LMK-235, and NMDA/PBS+MS-275. RGCs were immunolabeled using Brn3a (upper row). AcH3 immunolabeling is shown in the bottom row. Scale bar = 40 μm. **b** Quantification of AcH3 levels in the GCL injected as indicated. AcH3 levels in the NMDA-treated eye were normalized to the PBS control eye from the same animal. One-way ANOVA with Bonferroni's post hoc test for multiple comparisons. $n = 4$. PBS vs PBS+LMK-235, $p > 0.9999$; NMDA vs NMDA+LMK-235, $p > 0.9999$; PBS vs PBS+MS-275, $p = 0.7352$; NMDA vs NMDA+MS-275, $p > 0.9999$. **c** Quantification of RGCs injected as indicated. RGC numbers in the NMDA-treated eye were normalized to the mean number of RGCs in the PBS-treated eyes at d1. One-way ANOVA with Bonferroni's post hoc test for multiple comparisons. $n = 4$. PBS vs NMDA, $p = 0.0404$; PBS+LMK-235 vs NMDA+LMK-235, $p = 0.0110$; PBS+MS-275 vs NMDA+MS-275, $p = 0.0644$; NMDA vs NMDA+LMK-235, $p > 0.9999$; NMDA vs NMDA+MS-275, $p > 0.9999$. **d** Quantification of RGCs injected as indicated. One-way ANOVA with Bonferroni's post hoc test for multiple comparisons. $n = 4$. PBS vs NMDA, $p = 0.0403$; PBS+LMK-235 vs NMDA+LMK-235, $p = 0.0110$; PBS+MS-275 vs NMDA+MS-275, $p = 0.0647$; NMDA vs NMDA+LMK-235, $p > 0.9999$; NMDA vs NMDA+MS-275, $p > 0.9999$. **e** Quantification of RGCs injected with NMDA/PBS and NMDA/PBS + LMK-235 and MS-275 in combination. RGC numbers in the NMDA-treated eye were normalized to the mean number of RGCs in the PBS-treated eyes at d1. One-way ANOVA with Bonferroni's post hoc test for multiple comparisons. $n = 5$. PBS vs NMDA, $p > 0.0001$; PBS+LMK-235+MS-275 vs NMDA+LMK-235+MS-275, $p > 0.0001$; NMDA vs NMDA+LMK-235+MS-275, $p = 0.5129$. **f** Quantification of RGCs injected as indicated in **e**. One-way ANOVA with Bonferroni's post hoc test for multiple comparisons. $n = 5$. PBS vs NMDA, $p > 0.0001$; PBS+LMK-235+MS-275 vs NMDA+LMK-235+MS-275, $p > 0.0001$; NMDA vs NMDA+LMK-235+MS-275, $p = 0.5129$. Graphs represent mean ± SEM. $^{****}p < 0.0001$, $^{*}p < 0.05$

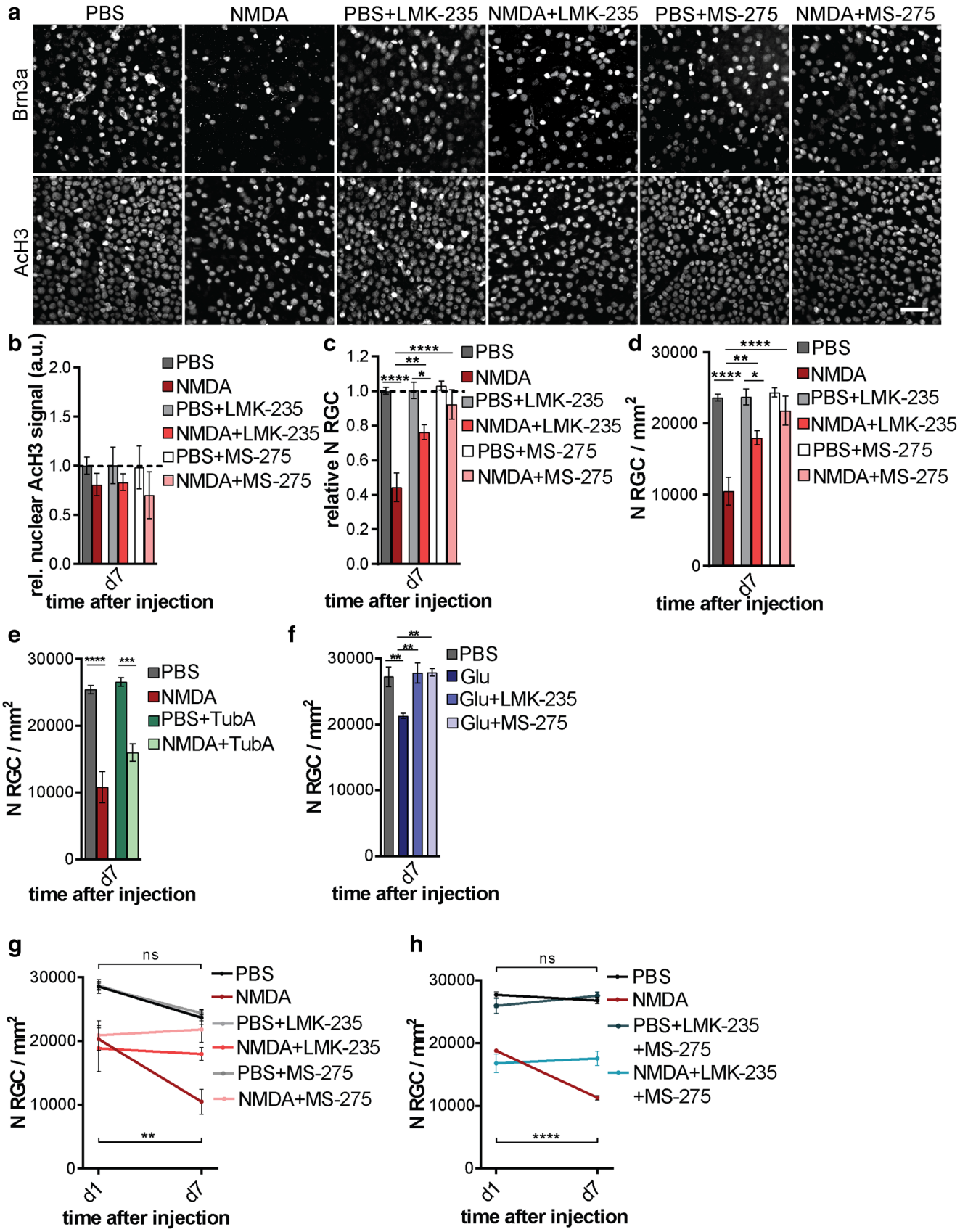
a
PBS
NMDA
PBS+LMK-235
NMDA+LMK-235
PBS+MS-275
NMDA+MS-275
Brn3a
AcH3
b
rel. nuclear AcH3 signal (a.u.)
time after injection
d7
c
relative N RGC
d
N RGC / mm²
e
PBS
NMDA
PBS+TubA
NMDA+TubA
f
Glu
Glu+LMK-235
Glu+MS-275
g
ns
d1
PBS+LMK-235 +MS-275
NMDA+LMK-235 +MS-275
h

◀ **Fig. 6** Inhibition of histone deacetylases attenuates NMDA-triggered excitotoxic retinal ganglion cell death at d7. **a** Representative images of retinal whole mounts at d7 after intravitreal injections of NMDA/PBS, NMDA/PBS+LMK-235, and NMDA/PBS+MS-275. RGCs were immunolabeled using Brn3a (upper row). AcH3 immunolabeling is shown in the bottom row. Scale bar = 40 μm. **b** Quantification of AcH3 levels injected as indicated. AcH3 levels in the NMDA-treated eye were normalized to the PBS control eye from the same animal. One-way ANOVA with Bonferroni's post hoc test for multiple comparisons. $n = 4$. PBS vs PBS+LMK-235, $p > 0.9999$; NMDA vs NMDA+LMK-235, $p > 0.9999$; PBS vs PBS+MS-275, $p > 0.9999$; NMDA vs NMDA+MS-275, $p > 0.9999$. **c** Quantification of RGCs injected as indicated. RGC numbers in the NMDA-treated eye were normalized to the mean number of RGCs in the PBS-treated eyes at d7. One-way ANOVA with Bonferroni's post hoc test for multiple comparisons. $n = 4$. PBS vs NMDA, $p < 0.0001$; PBS+LMK-235 vs NMDA+LMK-235, $p = 0.0376$; PBS+MS-275 vs NMDA+MS-275, $p = 0.9743$; NMDA vs NMDA+LMK-235, $p = 0.0047$; NMDA vs NMDA+MS-275, $p < 0.0001$. **d** Quantification of RGCs injected as indicated. One-way ANOVA with Bonferroni's post hoc test for multiple comparisons. $n = 4$. PBS vs NMDA, $p < 0.0001$; PBS+LMK-235 vs NMDA+LMK-235, $p = 0.0376$; PBS+MS-275 vs NMDA+MS-275, $p = 0.9707$; NMDA vs NMDA+LMK-235, $p = 0.0047$; NMDA vs NMDA+MS-275, $p < 0.0001$. **e** Quantification of RGCs injected with NMDA/PBS and NMDA/PBS + Tubastatin A (TubA). One-way ANOVA with Bonferroni's post hoc test for multiple comparisons. $n = 5$. PBS vs NMDA, $p > 0.0001$; PBS+TubA vs NMDA+TubA, $p = 0.0002$; NMDA vs NMDA+TubA, $p = 0.0590$. **f** Quantification of RGCs injected with glutamate (Glu)/PBS, Glu + LMK-235, and Glu + MS-275. One-way ANOVA with Bonferroni's post hoc test for multiple comparisons. $n = 5$. PBS vs Glu, $p = 0.0041$; Glu vs Glu+LMK-235, $p = 0.0019$; Glu vs Glu+MS-275, $p = 0.0010$; Glu+LMK-235 vs Glu+MS-275, $p > 0.9999$. **g** Time course analysis of progressive RGC death between d1 and d7 injected as indicated in **a**. Two-way ANOVA with Bonferroni's post hoc test for multiple comparisons. $n = 4$. PBS d1 vs d7, $p = 0.277$; NMDA d1 vs d7, $p = 0.0012$; PBS+LMK-235 d1 vs d7, $p = 0.2524$; NMDA+LMK-235 d1 vs d7, $p > 0.9999$; PBS+MS-275 d1 vs d7, $p = 0.5380$; NMDA+MS-275 d1 vs d7, $p > 0.9999$. **h** Time course analysis of progressive RGC death between d1 and d7 injected with NMDA/PBS and NMDA/PBS + LMK-235 and MS-275 in combination. Two-way ANOVA with Bonferroni's post hoc test for multiple comparisons. $n = 5$. PBS d1 vs d7, $p > 0.9999$; NMDA d1 vs d7, $p < 0.0001$; PBS+LMK-235+MS-275 d1 vs d7, $p = 0.8200$; NMDA+LMK-235+MS-275 d1 vs d7, $p > 0.9999$. Graphs/dots represent mean ± SEM. $^{****}p < 0.0001$, $^{***}p < 0.001$, $^{**}p < 0.01$, $^{*}p < 0.05$

Acetylation Levels of Histone 3 in Retinal Ganglion Cells Are Unaltered by NMDA-Triggered Excitotoxicity

HDACs catalyze histone protein deacetylation, a process implicated in early nuclear changes of RGCs in optic neuropathies and their apoptotic death [47]. We quantified the levels of acetylated histone H3 at lysine 9 (AcH3) as well as of total histone 3 (H3) in Brn3a-positive RGCs after the excitotoxic insult (Fig. 4). At d1 or d7 after NMDA intravitreal injection, AcH3 and H3 nuclear levels, as well as the AcH3/H3 ratio in Brn3a-positive RGCs, were unaltered as compared to PBS controls (Fig. 4 and data not shown).

HDAC Inhibition Attenuates NMDA-Triggered Excitotoxic Retinal Ganglion Cell Death

NMDA-triggered excitotoxicity causes RGC death in a time-dependent manner (Fig. 1) as well as altered subcellular localization of HDACs (Figs. 2 and 3). We sought to examine whether HDAC activity might be an underlying cause to RGC degeneration. Given the fact that excitotoxicity had the strongest and most consistent effects on HDAC4, HDAC5 (class IIa), and HDAC3 (class I), we decided to employ LMK-235 (N-((6-(hydroxyamino)-6-oxohexyl)oxy)-3,5-dimethylbenzamide) [31] and MS-275 (entinostat) [32] to inhibit HDAC4/5 or HDAC1–3, respectively [49, 50]. We delivered the inhibitors via intravitreal injection at the same time as NMDA and analyzed the eyes at d1 and d7 post-injections. One day after delivery, in comparison with PBS- or NMDA-injected eyes, the retinas of eyes injected with the inhibitors did not show statistically significant changes of AcH3 levels (Fig. 5a, b). Moreover, we could not detect any effect of both inhibitors on the NMDA-triggered RGC death (Fig. 5a, c–d). Even when delivered in combination, MS-275 and LMK-235 failed to protect RGCs from NMDA-triggered death (Fig. 5e, f; Supplementary Fig. 1A). Seven days after delivery, retinas from LMK-235 or MS-275 injected eyes did not show detectable increased levels of AcH3 in RGCs (Fig. 6a, b). Interestingly, both LMK-235- and MS-275-injected eyes showed significantly more Brn3a-positive RGCs in comparison with NMDA-only-injected eyes (Fig. 6a, c–d, g). Of the two inhibitors, MS-275 seemed to provide stronger protection against NMDA toxicity (Fig. 6a, c–d, g). Tubastatin A, a specific inhibitor of HDAC6 [51], whose subcellular localization was slightly altered at d1 and completely unaltered at d7 after intravitreal injection of NMDA (Figs. 2 and 3) did not spare RGCs from NMDA-induced degeneration (Fig. 6e). Both MS-275 and LMK-235 fully protected RGCs from death against intravitreal injection of glutamate, which is a milder insult in comparison with NMDA (Fig. 6f) [52, 53]. We reasoned that differences in the detected effects of MS-275 and LMK-235 at d7 and d1 could be due to the fact that, post-NMDA-mediated insult, RGCs continue to degenerate over time (Fig. 1). Thus, we compared the number of RGCs at d1 and d7 within experimental conditions. As expected, there was no significant difference in PBS-injected eyes between d1 and d7, while NMDA-injected eyes displayed time-dependent degeneration (Fig. 6g, h). Direct comparison between the quantified RGCs at d1 and d7 revealed that, while both inhibitors could not blunt the immediate NMDA-triggered death of RGCs (d1), they fully prevented the further degeneration of RGCs over time both when delivered alone (Fig. 6g, d7) and in a combinatorial approach (Fig. 6h, d7).

Discussion

In this work, we used an in vivo model of excitotoxicity to investigate HDACs in the degenerating murine neural retina. We found alterations in the subcellular localization of different HDACs in RGCs and that specific HDAC inhibition protects RGCs from ongoing degeneration.

Excitotoxicity underlies both acute and chronic disorders of the nervous system [54]. As regards the visual system, the sensitivity of RGCs to high glutamate and NMDA exposure was previously shown [41, 43, 55] and linked to several retinal disorders [16–20, 56]. Indeed, after a single NMDA intravitreal injection, we detected robust RGC loss, which significantly progressed over time. In addition, at the early d1 time point, but not at d7, we detected an increased number of fragmented nuclei in the GCL, an observation previously reported to be one of the early markers of RGC degeneration [47].

Epigenetics belong to the cellular and molecular events, which can be modulated by excitotoxicity and linked to acute and neurodegenerative diseases [57]. For instance, NMDA and glutamate promote nuclear accumulation of HDAC4 in hippocampal neurons, leading to their degeneration [13, 23]. Up to now, no detailed description of the effects of in vivo excitotoxicity on the different HDACs was available. Here, we characterized the subcellular localization of nine classical HDACs representative of classes I, IIa, IIb, and IV following in vivo excitotoxicity. All classes displayed changes after 24 h while, at a later time point (d7), HDAC4 and HDAC9 belonging to class IIa were the only affected HDACs.

Class IIa HDACs are the ones with the most defined capacity to shuttle between the cytoplasm and nucleus following external stimuli in a signal-dependent manner [4, 5, 14]. For HDAC4, this shuttling has been described to have roles in several neurodegenerative disorders [24, 26, 27]. Yet, there have been reports, showing subcellular redistribution also for non-class IIa HDACs. For instance, HDAC3 is primarily localized to the cytoplasm of RGCs [29, 58] but translocates to the nuclei of dying cells upon optic nerve lesion [29, 30]. A similar observation was made in a mouse model of Huntington's disease, in which HDAC3 progressively accumulates in the nucleus of cortical neurons [59]. Nuclear import of HDAC3 is suggested to induce heterochromatin formation and apoptosis in RGCs [47]. We detected increased nuclear HDAC3 levels, but not HDAC1, also belonging to class I, along with higher chromatin fragmentation and condensation at d1 after excitotoxicity. It would be valuable to assess if the RGCs displaying increased nuclear HDAC3 content are the ones further degenerating over time. Such hypothesis is supported by our observation that interfering with HDAC3 activity indeed blunts the progression of RGC degeneration and that reduced HDAC3 expression prevents nuclei condensation and RGC degeneration [30]. HDAC6 is mainly found in the cytoplasm of neurons [60]; however, in non-neuronal cells, it was reported to shuttle between the cytoplasm and nucleus [61, 62]. Our experiments showed increased nuclear levels of HDAC6 in RGCs 1 day after the NMDA-triggered excitotoxic insult. HDAC6 activity, however, does not seem to play a role in RGC degeneration as its inhibition did not prevent the NMDA-mediated loss of RGCs. We additionally detected a decrease in nuclear HDAC11, for which a shuttling activity has so far not been reported. Seven days after the NMDA-triggered excitotoxic insult, only class IIa HDAC subcellular localization was altered. It remains to be determined if such changes might be critical at even later stages. In our model, we did not detect any significant changes in the global acetylation levels of histone 3 following NMDA intravitreal injection. This could be due to the fact that, overall, HDACs displayed bidirectional shuttling with some showing increased while others decreased nuclear content. Moreover, we cannot exclude the possibility that other lysine residues on histone 3 or different histones as well as non-histone proteins might be affected [3]. Future experiments should focus on locus-specific alterations in the acetylation pattern, and it would be interesting to determine which specific genes, under the control of the different HDACs, might be critical in the modulation of RGC excitotoxic degeneration. Alterations in the RGC gene expression profile prior to their death have been reported and associated with HDAC activation state [63]. The affected genes included also known markers used for the identification of RGCs. We cannot completely rule out the possibility that the reduced levels of Brn3a, the marker we used for RGC quantification, might be predominantly related to alterations of transcription, possibly modulated by HDACs, rather than to an actual reduction in the number of RGCs. However, we consistently observed a reduction in the number of nuclei in the GCL and several studies reported a loss of RGCs following excitotoxicity using methods not relying on markers [64, 65], supporting the idea that RGCs are indeed degenerating. Moreover, we detected a persistent NMDA-mediated down-regulation of the RGC markers *Thy1* and *Nefl*, accompanied by transient changes in the mRNA levels of *Actb*, *Atf3*, *Bdnf*, and *Arc*. It is well-known that NMDA-mediated excitotoxicity modulates expression of a large pool of genes [22], consistent with our observations relative to 1 day post-NMDA treatment. At a later time point, however, the only affected genes by NMDA-mediated injury remained the RGC markers *Thy1* and *Nefl* while the mRNA level of all other analyzed genes was not changed.

In recent years, HDACs have received increasing attention as potential targets for the treatment of several diseases [66]. Several HDAC inhibitors have been and still are under evaluation in clinical trials [67]. The use of pan-inhibitors of HDACs, such as valproic acid (VPA) and Trichostatin A (TSA), is accompanied by side effects and might thus not represent the best therapeutic strategy [68, 69]. Therefore, it is critical to gather information on the activity, function, and inhibition of the individual HDACs. In the retina, pan-HDAC inhibitors displayed some degree of protection of RGCs from degeneration after optic nerve crush [29, 70], retinal ischemia [71], and glaucoma [72, 73].

Here, we targeted the activity of HDAC3 and HDAC4/5, which showed the strongest excitotoxicity-induced alterations (Figs. 2 and 3), with the selective inhibitors MS-275 (HDAC1–3) and LMK-235 (HDAC4/5). Our data show that both inhibitors significantly blunt the excitotoxic degeneration over time of RGCs while they cannot spare RGCs from the initial toxic events caused by NMDA. Even the combined delivery of these inhibitors could not spare RGCs in the acute phase. Different doses of inhibitors or their delivery prior to the insult might prove beneficial under acute conditions. It should also be considered that the NMDA-based insult results particularly harsh causing a loss of RGCs of up to 60%. Both inhibitors displayed higher protective capacities against a milder insult, based on glutamate intravitreal delivery, which causes less damage to RGCs [52, 53]. The fact that we prevented time-dependent degeneration is particularly interesting in light of potential clinical applications. In line with our observations, protective properties of MS-275 following optic nerve injury, in animal models of multiple sclerosis and traumatic brain injury as well as during aging have been reported [74–77]. LMK-235 has been prevalently tested for potential cancer therapies [31, 78]. LMK-235 successfully counteracted neurodevelopmental abnormalities in a mouse model of *CDKL5* disorder characterized by augmented content of HDAC4 in the nucleus [79] but has not yet been tested for its neuroprotective properties. Since increased nuclear levels of HDAC4 in neurons have been linked to many neurodegenerative conditions, it would be interesting to evaluate the efficacy of LMK-235 in such disorders [24–28].

In conclusion, our study characterized the specific effects of in vivo excitotoxicity on different HDACs in RGCs and suggests that selective inhibitors of HDACs might be beneficial in the treatments of neurodegenerative disorders.

Acknowledgments The authors thank Dr. Bettina Buchthal for her help with the establishment of intravitreal injections. DM is a member of the Excellence Cluster *CellNetworks* at Heidelberg University. Part of the pictures was acquired at the Nikon Imaging Center at Heidelberg University.

Funding Information This work was supported by the FOR2325 grant (project 2) and SFB1158 (project A08) of the Deutsche Forschungsgemeinschaft (DFG) to DM, the FRONTIER grant of Heidelberg University to DM, Italian PRIN 2016 (prot. 20152TE5PK to AM), AIRC 2016 (n. 19162 to AM), and PE-2013-02355271 to AM.

Compliance with Ethical Standards

This article does not contain any studies with human participants performed by any of the authors. All procedures performed in studies involving animals were in accordance with the ethical standards of the institution or practice at which the studies were conducted. All procedures were approved by the local governing body for animal welfare (Regierungspräsidium Karlsruhe).

Conflict of Interest The authors declare no potential conflicts of interest with respect to the research, authorship, and/or publication of this article. DM is one of the founders and shareholders of FundaMental Pharma GmbH.

References

1. Bannister AJ, Kouzarides T (2011) Regulation of chromatin by histone modifications. Cell Res 21(3):381–395. https://doi.org/10.1038/cr.2011.22
2. Peserico A, Simone C (2011) Physical and functional HAT/HDAC interplay regulates protein acetylation balance. J Biomed Biotechnol 2011:371832. https://doi.org/10.1155/2011/371832
3. Seto E, Yoshida M (2014) Erasers of histone acetylation: the histone deacetylase enzymes. Cold Spring Harb Perspect Biol 6(4): a018713. https://doi.org/10.1101/cshperspect.a018713
4. Haberland M, Montgomery RL, Olson EN (2009) The many roles of histone deacetylases in development and physiology: implications for disease and therapy. Nat Rev Genet 10(1):32–42. https://doi.org/10.1038/nrg2485
5. Clocchiatti A, Florean C, Brancolini C (2011) Class IIa HDACs: from important roles in differentiation to possible implications in tumourigenesis. J Cell Mol Med 15(9):1833–1846. https://doi.org/10.1111/j.1582-4934.2011.01321.x
6. Lee YS, Lim KH, Guo X, Kawaguchi Y, Gao Y, Barrientos T, Ordentlich P, Wang XF et al (2008) The cytoplasmic deacetylase HDAC6 is required for efficient oncogenic tumorigenesis. Cancer Res 68(18):7561–7569. https://doi.org/10.1158/0008-5472.can-08-0188
7. Tong JJ, Liu J, Bertos NR, Yang XJ (2002) Identification of HDAC10, a novel class II human histone deacetylase containing a leucine-rich domain. Nucleic Acids Res 30(5):1114–1123
8. Bazou D, Ng MR, Song JW, Chin SM, Maimon N, Munn LL (2016) Flow-induced HDAC1 phosphorylation and nuclear export in angiogenic sprouting. Sci Rep 6:34046. https://doi.org/10.1038/srep34046
9. Riolo MT, Cooper ZA, Holloway MP, Cheng Y, Bianchi C, Yakirevich E, Ma L, Chin YE et al (2012) Histone deacetylase 6 (HDAC6) deacetylates survivin for its nuclear export in breast cancer. J Biol Chem 287(14):10885–10893. https://doi.org/10.1074/jbc.M111.308791
10. Winkler AR, Nocka KN, Williams CM (2012) Smoke exposure of human macrophages reduces HDAC3 activity, resulting in enhanced inflammatory cytokine production. Pulm Pharmacol Ther 25(4):286–292. https://doi.org/10.1016/j.pupt.2012.05.003
11. Yang Y, Huang Y, Wang Z, Wang HT, Duan B, Ye D, Wang C, Jing R et al (2016) HDAC10 promotes lung cancer proliferation via AKT phosphorylation. Oncotarget 7(37):59388–59401. https://doi.org/10.18632/oncotarget.10673
12. Zhao X, Ito A, Kane CD, Liao TS, Bolger TA, Lemrow SM, Means AR, Yao TP (2001) The modular nature of histone deacetylase HDAC4 confers phosphorylation-dependent intracellular trafficking. J Biol Chem 276(37):35042–35048. https://doi.org/10.1074/jbc.M105086200
13. Chawla S, Vanhoutte P, Arnold FJ, Huang CL, Bading H (2003) Neuronal activity-dependent nucleocytoplasmic shuttling of HDAC4 and HDAC5. J Neurochem 85(1):151–159
14. Schlumm F, Mauceri D, Freitag HE, Bading H (2013) Nuclear calcium signaling regulates nuclear export of a subset of class IIa histone deacetylases following synaptic activity. J Biol Chem 288(12):8074–8084. https://doi.org/10.1074/jbc.M112.432773
15. Hardingham GE, Bading H (2010) Synaptic versus extrasynaptic NMDA receptor signalling: Implications for neurodegenerative disorders. Nat Rev Neurosci 11(10):682–696. https://doi.org/10.1038/nrn2911
16. Casson RJ (2006) Possible role of excitotoxicity in the pathogenesis of glaucoma. Clin Exp Ophthalmol 34(1):54–63. https://doi.org/10.1111/j.1442-9071.2006.01146.x
17. Dreyer EB (1998) A proposed role for excitotoxicity in glaucoma. J Glaucoma 7(1):62–67

18. Dreyer EB, Zurakowski D, Schumer RA, Podos SM, Lipton SA (1996) Elevated glutamate levels in the vitreous body of humans and monkeys with glaucoma. Archi Ophthalmol (Chicago, Ill : 1960) 114(3):299–305
19. Hernandez C, Simo R (2012) Neuroprotection in diabetic retinopathy. Curr Diab Rep 12(4):329–337. https://doi.org/10.1007/s11892-012-0284-5
20. Opere CA, Heruye S, Njie-Mbye YF, Ohia SE, Sharif NA (2018) Regulation of excitatory amino acid transmission in the retina: studies on neuroprotection. J Ocul Pharmacol Ther 34(1–2):107–118. https://doi.org/10.1089/jop.2017.0085
21. Hardingham GE, Fukunaga Y, Bading H (2002) Extrasynaptic NMDARs oppose synaptic NMDARs by triggering CREB shut-off and cell death pathways. Nat Neurosci 5(5):405–414. https://doi.org/10.1038/nn835.nn835
22. Zhang SJ, Steijaert MN, Lau D, Schutz G, Delucinge-Vivier C, Descombes P, Bading H (2007) Decoding NMDA receptor signaling: identification of genomic programs specifying neuronal survival and death. Neuron 53(4):549–562. https://doi.org/10.1016/j.neuron.2007.01.025
23. Litke C, Bading H, Mauceri D (2018) Histone deacetylase 4 shapes neuronal morphology via a mechanism involving regulation of expression of vascular endothelial growth factor D. J Biol Chem 293(21):8196–8207. https://doi.org/10.1074/jbc.RA117.001613
24. Kassis H, Shehadah A, Chopp M, Roberts C, Zhang ZG (2015) Stroke induces nuclear shuttling of histone deacetylase 4. Stroke 46(7):1909–1915. https://doi.org/10.1161/strokeaha.115.009046
25. Shen X, Chen J, Li J, Kofler J, Herrup K (2016) Neurons in vulnerable regions of the Alzheimer's disease brain display reduced ATM signaling. eNeuro 3(1). https://doi.org/10.1523/ENEURO.0124-15.2016
26. Wu Q, Yang X, Zhang L, Zhang Y, Feng L (2017) Nuclear accumulation of histone deacetylase 4 (HDAC4) exerts neurotoxicity in models of Parkinson's disease. Mol Neurobiol 54(9):6970–6983. https://doi.org/10.1007/s12035-016-0199-2
27. Yuan H, Denton K, Liu L, Li XJ, Benashski S, McCullough L, Li J (2016) Nuclear translocation of histone deacetylase 4 induces neuronal death in stroke. Neurobiol Dis 91:182–193. https://doi.org/10.1016/j.nbd.2016.03.004
28. Li J, Chen J, Ricupero CL, Hart RP, Schwartz MS, Kusnecov A, Herrup K (2012) Nuclear accumulation of HDAC4 in ATM deficiency promotes neurodegeneration in ataxia telangiectasia. Nat Med 18(5):783–790. https://doi.org/10.1038/nm.2709
29. Pelzel HR, Schlamp CL, Nickells RW (2010) Histone H4 deacetylation plays a critical role in early gene silencing during neuronal apoptosis. BMC Neurosci 11:62. https://doi.org/10.1186/1471-2202-11-62
30. Schmitt HM, Pelzel HR, Schlamp CL, Nickells RW (2014) Histone deacetylase 3 (HDAC3) plays an important role in retinal ganglion cell death after acute optic nerve injury. Mol Neurodegener 9:39. https://doi.org/10.1186/1750-1326-9-39
31. Marek L, Hamacher A, Hansen FK, Kuna K, Gohlke H, Kassack MU, Kurz T (2013) Histone deacetylase (HDAC) inhibitors with a novel connecting unit linker region reveal a selectivity profile for HDAC4 and HDAC5 with improved activity against chemoresistant cancer cells. J Med Chem 56(2):427–436. https://doi.org/10.1021/jm301254q
32. Suzuki T, Ando T, Tsuchiya K, Fukazawa N, Saito A, Mariko Y, Yamashita T, Nakanishi O (1999) Synthesis and histone deacetylase inhibitory activity of new benzamide derivatives. J Med Chem 42(15):3001–3003. https://doi.org/10.1021/jm980565u
33. Choi SY, Kee HJ, Kurz T, Hansen FK, Ryu Y, Kim GR, Lin MQ, Jin L et al (2016) Class I HDACs specifically regulate E-cadherin expression in human renal epithelial cells. J Cell Mol Med 20(12):2289–2298. https://doi.org/10.1111/jcmm.12919
34. Jaboin J, Wild J, Hamidi H, Khanna C, Kim CJ, Robey R, Bates SE, Thiele CJ (2002) MS-27-275, an inhibitor of histone deacetylase, has marked in vitro and in vivo antitumor activity against pediatric solid tumors. Cancer Res 62(21):6108–6115
35. Kaplan HJ, Chiang CW, Chen J, Song SK (2010) Vitreous volume of the mouse measured by quantitative high-resolution MRI. Invest Ophthalmol Vis Sci 51(13):4414–4414
36. Guo W, Naujock M, Fumagalli L, Vandoorne T, Baatsen P, Boon R, Ordovas L, Patel A et al (2017) HDAC6 inhibition reverses axonal transport defects in motor neurons derived from FUS-ALS patients. Nat Commun 8(1):861. https://doi.org/10.1038/s41467-017-00911-y
37. Depetter Y, Geurs S, De Vreese R, Goethals S, Vandoorn E, Laevens A, Steenbrugge J, Meyer E et al (2019) Selective pharmacological inhibitors of HDAC6 reveal biochemical activity but functional tolerance in cancer models. Int J Cancer. https://doi.org/10.1002/ijc.32169
38. Sen A, Nelson TJ, Alkon DL (2015) ApoE4 and Abeta oligomers reduce BDNF expression via HDAC nuclear translocation. J Neurosci 35(19):7538–7551. https://doi.org/10.1523/jneurosci.0260-15.2015
39. Sucher NJ, Lipton SA, Dreyer EB (1997) Molecular basis of glutamate toxicity in retinal ganglion cells. Vis Res 37(24):3483–3493. https://doi.org/10.1016/S0042-6989(97)00047-3
40. Shen Y, Liu XL, Yang XL (2006) N-Methyl-D-aspartate receptors in the retina. Mol Neurobiol 34(3):163–179. https://doi.org/10.1385/MN:34:3:163
41. Lebrun-Julien F, Duplan L, Pernet V, Osswald I, Sapieha P, Bourgeois P, Dickson K, Bowie D et al (2009) Excitotoxic death of retinal neurons in vivo occurs via a non-cell-autonomous mechanism. J Neurosci 29(17):5536–5545. https://doi.org/10.1523/JNEUROSCI.0831-09.2009
42. Li Y, Schlamp CL, Nickells RW (1999) Experimental induction of retinal ganglion cell death in adult mice. Invest Ophthalmol Vis Sci 40(5):1004–1008
43. Nakanishi N, Tu S, Shin Y, Cui J, Kurokawa T, Zhang D, Chen HS, Tong G et al (2009) Neuroprotection by the NR3A subunit of the NMDA receptor. J Neurosci 29(16):5260–5265. https://doi.org/10.1523/JNEUROSCI.1067-09.2009
44. Xiang M, Zhou L, Macke JP, Yoshioka T, Hendry SH, Eddy RL, Shows TB, Nathans J (1995) The Brn-3 family of POU-domain factors: primary structure, binding specificity, and expression in subsets of retinal ganglion cells and somatosensory neurons. J Neurosci 15(7 Pt 1):4762–4785
45. Cummings BS, Wills LP, Schnellmann RG (2012) Measurement of cell death in mammalian cells. Curr Protoc Pharmacol Chapter12: Unit12 18. https://doi.org/10.1002/0471141755.ph1208s56
46. Daly C, Yin J, Kennedy BN (2016) Histone deacetylase: therapeutic targets in retinal degeneration. Adv Exp Med Biol 854:455–461. https://doi.org/10.1007/978-3-319-17121-0_61
47. Schmitt HM, Schlamp CL, Nickells RW (2016) Role of HDACs in optic nerve damage-induced nuclear atrophy of retinal ganglion cells. Neurosci Lett 625:11–15. https://doi.org/10.1016/j.neulet.2015.12.012
48. Saha A, Tiwari S, Dharmarajan S, Otteson DC, Belecky-Adams TL (2018) Class I histone deacetylases in retinal progenitors and differentiating ganglion cells. Gene Expr Patterns 30:37–48. https://doi.org/10.1016/j.gep.2018.08.007
49. Khan N, Jeffers M, Kumar S, Hackett C, Boldog F, Khramtsov N, Qian X, Mills E et al (2008) Determination of the class and isoform selectivity of small-molecule histone deacetylase inhibitors. Biochem J 409(2):581–589. https://doi.org/10.1042/BJ20070779
50. Hess-Stumpp H, Bracker TU, Henderson D, Politz O (2007) MS-275, a potent orally available inhibitor of histone deacetylases–the development of an anticancer agent. Int J Biochem Cell Biol 39(7–8):1388–1405. https://doi.org/10.1016/j.biocel.2007.02.009
51. Butler KV, Kalin J, Brochier C, Vistoli G, Langley B, Kozikowski AP (2010) Rational design and simple chemistry yield a superior, neuroprotective HDAC6 inhibitor, tubastatin A. J Am Chem Soc 132(31):10842–10846. https://doi.org/10.1021/ja102758v

52. Schori H, Kipnis J, Yoles E, WoldeMussie E, Ruiz G, Wheeler LA, Schwartz M (2001) Vaccination for protection of retinal ganglion cells against death from glutamate cytotoxicity and ocular hypertension: implications for glaucoma. Proc Natl Acad Sci U S A 98(6):3398–3403. https://doi.org/10.1073/pnas.041609498
53. Schori H, Yoles E, Schwartz M (2001) T-cell-based immunity counteracts the potential toxicity of glutamate in the central nervous system. J Neuroimmunol 119(2):199–204
54. Bading H (2017) Therapeutic targeting of the pathological triad of extrasynaptic NMDA receptor signaling in neurodegenerations. J Exp Med 214(3):569–578. https://doi.org/10.1084/jem.20161673
55. Schmidt KG, Bergert H, Funk RH (2008) Neurodegenerative diseases of the retina and potential for protection and recovery. Curr Neuropharmacol 6(2):164–178. https://doi.org/10.2174/157015908784533851
56. Pitt D, Werner P, Raine CS (2000) Glutamate excitotoxicity in a model of multiple sclerosis. Nat Med 6(1):67–70. https://doi.org/10.1038/71555
57. Hwang JY, Aromolaran KA, Zukin RS (2017) The emerging field of epigenetics in neurodegeneration and neuroprotection. Nat Rev Neurosci 18(6):347–361. https://doi.org/10.1038/nrn.2017.46
58. Fan J, Alsarraf O, Dahrouj M, Platt KA, Chou CJ, Rice DS, Crosson CE (2013) Inhibition of HDAC2 protects the retina from ischemic injury. Invest Ophthalmol Vis Sci 54(6):4072–4080. https://doi.org/10.1167/iovs.12-11529
59. Jia H, Pallos J, Jacques V, Lau A, Tang B, Cooper A, Syed A, Purcell J et al (2012) Histone deacetylase (HDAC) inhibitors targeting HDAC3 and HDAC1 ameliorate polyglutamine-elicited phenotypes in model systems of Huntington's disease. Neurobiol Dis 46(2):351–361
60. Govindarajan N, Rao P, Burkhardt S, Sananbenesi F, Schluter OM, Bradke F, Lu J, Fischer A (2013) Reducing HDAC6 ameliorates cognitive deficits in a mouse model for Alzheimer's disease. EMBO Mol Med 5(1):52–63. https://doi.org/10.1002/emmm.201201923
61. Liu Y, Peng L, Seto E, Huang S, Qiu Y (2012) Modulation of histone deacetylase 6 (HDAC6) nuclear import and tubulin deacetylase activity through acetylation. J Biol Chem 287(34):29168–29174. https://doi.org/10.1074/jbc.M112.371120
62. Verdel A, Curtet S, Brocard MP, Rousseaux S, Lemercier C, Yoshida M, Khochbin S (2000) Active maintenance of mHDA2/mHDAC6 histone-deacetylase in the cytoplasm. Curr Biol: CB 10(12):747–749
63. Pelzel HR, Nickells RW (2011) A role for epigenetic changes in the development of retinal neurodegenerative conditions. J Ocul Biol Dis Infor 4(3):104–110. https://doi.org/10.1007/s12177-012-9079-9
64. Hama Y, Katsuki H, Tochikawa Y, Suminaka C, Kume T, Akaike A (2006) Contribution of endogenous glycine site NMDA agonists to excitotoxic retinal damage in vivo. Neurosci Res 56(3):279–285. https://doi.org/10.1016/j.neures.2006.07.008
65. Pernet V, Bourgeois P, Di Polo A (2007) A role for polyamines in retinal ganglion cell excitotoxic death. J Neurochem 103(4):1481–1490. https://doi.org/10.1111/j.1471-4159.2007.04843.x
66. Didonna A, Opal P (2015) The promise and perils of HDAC inhibitors in neurodegeneration. Ann Clin Transl Neurol 2(1):79–101. https://doi.org/10.1002/acn3.147
67. Hadden MJ, Advani A (2018) Histone deacetylase inhibitors and diabetic kidney disease. Int J Mol Sci 19(9). https://doi.org/10.3390/ijms19092630
68. Ceccacci E, Minucci S (2016) Inhibition of histone deacetylases in cancer therapy: lessons from leukaemia. Br J Cancer 114(6):605–611. https://doi.org/10.1038/bjc.2016.36
69. Subramanian S, Bates SE, Wright JJ, Espinoza-Delgado I, Piekarz RL (2010) Clinical toxicities of histone deacetylase inhibitors. Pharmaceuticals (Basel, Switzerland) 3(9):2751–2767. https://doi.org/10.3390/ph3092751
70. Biermann J, Grieshaber P, Goebel U, Martin G, Thanos S, Di Giovanni S, Lagreze WA (2010) Valproic acid-mediated neuroprotection and regeneration in injured retinal ganglion cells. Invest Ophthalmol Vis Sci 51(1):526–534. https://doi.org/10.1167/iovs.09-3903
71. Crosson CE, Mani SK, Husain S, Alsarraf O, Menick DR (2010) Inhibition of histone deacetylase protects the retina from ischemic injury. Invest Ophthalmol Vis Sci 51(7):3639–3645. https://doi.org/10.1167/iovs.09-4538
72. Alsarraf O, Fan J, Dahrouj M, Chou CJ, Yates PW, Crosson CE (2014) Acetylation preserves retinal ganglion cell structure and function in a chronic model of ocular hypertension. Invest Ophthalmol Vis Sci 55(11):7486–7493. https://doi.org/10.1167/iovs.14-14792
73. Pelzel HR, Schlamp CL, Waclawski M, Shaw MK, Nickells RW (2012) Silencing of Fem1cR3 gene expression in the DBA/2J mouse precedes retinal ganglion cell death and is associated with histone deacetylase activity. Invest Ophthalmol Vis Sci 53(3):1428–1435. https://doi.org/10.1167/iovs.11-8872
74. Chindasub P, Lindsey JD, Duong-Polk K, Leung CK, Weinreb RN (2013) Inhibition of histone deacetylases 1 and 3 protects injured retinal ganglion cells. Invest Ophthalmol Vis Sci 54(1):96–102. https://doi.org/10.1167/iovs.12-10850
75. Kim JY, Shen S, Dietz K, He Y, Howell O, Reynolds R, Casaccia P (2010) HDAC1 nuclear export induced by pathological conditions is essential for the onset of axonal damage. Nat Neurosci 13(2):180–189. https://doi.org/10.1038/nn.2471
76. Cao P, Liang Y, Gao X, Zhao MG, Liang GB (2013) Administration of MS-275 improves cognitive performance and reduces cell death following traumatic brain injury in rats. CNS Neurosci Ther 19(5):337–345. https://doi.org/10.1111/cns.12082
77. Baltan S (2012) Histone deacetylase inhibitors preserve function in aging axons. J Neurochem 123(Suppl 2):108–115. https://doi.org/10.1111/j.1471-4159.2012.07949.x
78. Kaletsch A, Pinkerneil M, Hoffmann MJ, Jaguva Vasudevan AA, Wang C, Hansen FK, Wiek C, Hanenberg H et al (2018) Effects of novel HDAC inhibitors on urothelial carcinoma cells. Clin Epigenetics 10(1):100. https://doi.org/10.1186/s13148-018-0531-y
79. Trazzi S, Fuchs C, Viggiano R, De Franceschi M, Valli E, Jedynak P, Hansen FK, Perini G et al (2016) HDAC4: a key factor underlying brain developmental alterations in CDKL5 disorder. Hum Mol Genet 25(18):3887–3907. https://doi.org/10.1093/hmg/ddw231